University of Groningen

The secular evolution of the Kuiper belt after a close stellar encounter

Punzo, D.; Capuzzo-Dolcetta, R.; Portegies Zwart, S.

IMPORTANT NOTE: You are advised to consult the publisher's version (publisher's PDF) if you wish to cite from it. Please check the document version below.

Document Version
Publisher's PDF, also known as Version of record

Link to publication in University of Groningen/UMCG research database

The secular evolution of the Kuiper belt after a close stellar encounter

D. Punzo,[1,2]⋆ R. Capuzzo-Dolcetta[1] and S. Portegies Zwart[3]

[1]*Department of Physics, Sapienza, University of Roma, P.le A. Moro 1, I-00185, Roma, Italy*
[2]*Kapteyn Institute, Rijksuniversiteit, Landleven 12, NL-9747AD Groningen, the Netherlands*
[3]*Leiden Observatory, Leiden University, PO Box 9513, NL-2300 RA Leiden, the Netherlands*

ABSTRACT

We show the effects of the perturbation caused by a passing by star on the Kuiper belt objects (KBOs) of our Solar system. The dynamics of the Kuiper belt (KB) is followed by direct *N*-body simulations. The sampling of the KB has been done with *N* up to 131 062, setting the KBOs on initially nearly circular orbits distributed in a ring of surface density $\Sigma \sim r^{-2}$. This modellization allowed us to investigate the secular evolution of the KB upon the encounter with the perturbing star. Actually, the encounter itself usually leads towards eccentricity and inclination distributions similar to observed ones, but tends also to excite the low-eccentricity population ($e \lesssim 0.1$ around $a \sim 40$ au from the Sun), depleting this region of low eccentricities. The following long-term evolution shows a 'cooling' of the eccentricities repopulating the low-eccentricity area. In dependence on the assumed KBO mass spectrum and sampled number of bodies, this repopulation takes place in a time that goes from 0.5 to 100 Myr. Due to the unavoidable limitation in the number of objects in our long-term simulations ($N \leq 16\,384$), we could not consider a detailed KBO mass spectrum, accounting for low-mass objects, thus our present simulations are not reliable in constraining correlations among inclination distribution of the KBOs and other properties, such as their size distribution. However, our high-precision long-term simulations are a starting point for future larger studies on massively parallel computational platforms which will provide a deeper investigation of the secular evolution (~ 100 Myr) of the KB over its whole mass spectrum.

Key words: methods: numerical – Kuiper belt: general – planets and satellites: dynamical evolution and stability.

1 INTRODUCTION

The Solar system is hedged by a ring composed of a huge number of small bodies: the Edgeworth–Kuiper belt (Jewitt & Luu 1993, hereafter briefly called Kuiper belt, or KB). The Kuiper belt bears the signature of the early evolution of the Solar system, and contains records of the end-state of the accretion processes occurred in that region. Therefore, the knowledge of the history of the Kuiper belt objects (KBOs) is relevant to be able to develop a full consensus of the formation of the Solar system.

The majority of the KBOs are located between about 30 and 90 au from the Sun, but most are around the 2:3 resonance with Jupiter, at 39.5 au and at its 1:2 resonance, roughly around 48 au. The total mass is estimated from 0.01 to 0.1 M⊕ (Luu & Jewitt 2002). There are several, indirect, arguments suggesting that this is just a small fraction of its initial mass because most of it has been lost (see Kenyon & Luu 1999). The size distribution of the KBOs is, usually,

assumed as a power law $dn/dR = AR^{-q}$, where A and q are constants. The q exponent is estimated $\sim 4.0 \pm 0.5$ (Bernstein et al. 2004; Fraser & Kavelaars 2009). For a more detailed description of the Kuiper belt we refer, e.g., to Luu & Jewitt (2002).

The KB has a bimodal inclination distribution resulting of two separate populations (Brown 2001). The *dynamically cold* population refers to objects moving on almost planar orbits with relatively low inclinations (up to about 10°) with respect to the ecliptic. On the other side, the dynamically hot population is characterized by highly inclined orbits (up to 40°) with respect to the ecliptic. Note that these two populations are different from what we call, in this paper, the *low-eccentricity* population, which are objects on nearly circular orbits (orbital eccentricities <0.1) and the *high-eccentricity* population (eccentricities $\gtrsim 0.1$).

In Fig. 1, the eccentricities and inclinations are plotted as function of the semimajor axis for KBOs observed from the Minor Planet Center (MPC; Marsden 1980) which is the centre of the Smithsonian Astrophysical Observatory dedicated to tracking, monitoring, calculating and disseminating data from asteroids and comets.

⋆ E-mail: D.Punzo@astro.rug.nl
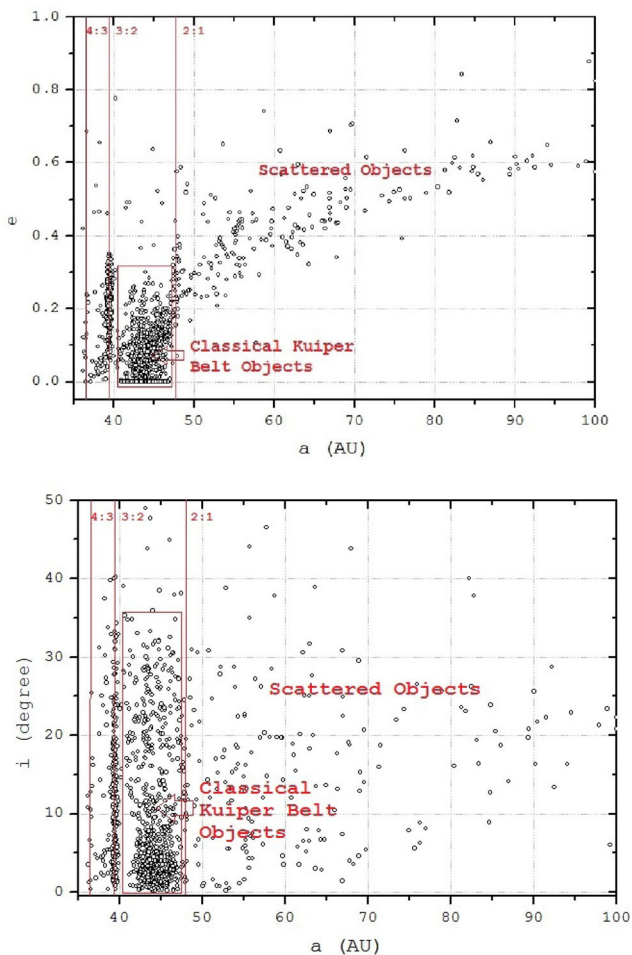
Figure 1. Distribution of the eccentricities (top panel) and inclinations (bottom panel) as a function of semimajor axis of the observed KBOs; data are from the MPC (Marsden 1980). The vertical lines highlight the main resonances.

The KBOs have been subcategorized in three groups:

(i) classical KBOs ($42 < a < 49$, $\langle e \rangle \simeq 0.09$, $\langle i \rangle \simeq 7°$);
(ii) scattered KBOs ($a > 30$, $\langle e \rangle \simeq 0.49$, $\langle i \rangle \simeq 14°$);
(iii) main resonant KBOs:

(a) 4:3 resonance ($a \simeq 36, 4$, $\langle e \rangle \simeq 0.22$, $\langle i \rangle \simeq 8°$);
(b) 3:2 resonance, Plutino's ($a \simeq 39.4$, $\langle e \rangle \simeq 0.36$, $\langle i \rangle \simeq 13°$);
(c) 2:1 resonance ($a \simeq 47.8$, $\langle e \rangle \simeq 0.14$, $\langle i \rangle \simeq 10°$),

where semimajor axes, a, are in au.

These subpopulations have been explained through a phase of planet migration and a phase of clearing of the environment during the evolution of the early Solar system (Malhotra 1993, 1995). In the latter phase, the resonant population was formed by sweeping resonance capture in which the Jovian planets withstand considerable orbital migration as a result of encounters with residual planetesimals. While Neptune moved outwards, a small body like Pluto in an initially circular orbit could have been captured into the 3:2 resonance. The high orbital eccentricity would subsequently be induced by repeated orbital crossings with Neptune.

Many others studies have attempted to better understand the properties of the KBOs. Gomes (2003) investigated how the outward migration of Neptune, as proposed by Malhotra (1993, 1995), could have scattered objects from 25 au on to high-i orbits leading

to the current classical Kuiper belt region. He concluded that the high-*i* population was formed closer to the Sun and brought into the classical Kuiper belt during planetary migration, whereas the cold population represents a primordial, relatively undisturbed population. This also led to the speculation that other mechanisms, such as planetary migration, have been the cause of the correlation between inclinations and colours in the classical Kuiper belt rather than environmental effects like the collisions among the KBOs (see Doressoundiram et al. 2008). Detailed discussions about the correlation of the inclination with the colour, size and binary of the KBOs are given by Levison & Stern (2001), Brucker et al. (2009), Noll et al. (2008) and Volk & Malhotra (2011). More recently a model, called the Nice model, has been proposed (Levison et al. 2008), which argues that the giant planets migrated from an initial compact configuration into their present orbits, long after the dissipation of the initial protoplanetary gas disc. The Nice model seems to provide an acceptable explanation for the formation of the classical and scattered populations, and for the correlation between inclinations and colours (for more details see Levison et al. 2008). The Nice model, however, predicts higher eccentricities in classical KBO orbits than is observed.

An interaction between a passing field star and the Solar system could also be responsible for some of the orbital families observed in the KBO, which is the main topic of this paper.

2 THE FLY-BY STAR PERTURBATION AND THE *N*-BODY SCHEME

An encounter between a passing star and the Solar system is quite likely, considering that the Solar system was probably formed in an open star cluster (Portegies Zwart 2009). The hypothesis of a closely passing star has been hypothesized before, and used to explain KBO families (Ida, Larwood & Burkert 2000; Kobayashi & Ida 2001; Kobayashi, Ida & Tanaka 2005; Melita, Larwood & Williams 2005; Malmberg, Davies & Heggie 2011). The cost of such calculations, however, prevented earlier research on the secular evolution of the KBO by means of high-resolution simulations.

We focus our attention on the investigation of the effects of the long-term evolution of the Kuiper belt after a close stellar encounter on the structure of the Kuiper belt. We adopt a direct *N*-body treatment in which the mutual, pairwise, interactions between KBOs, planets and stars are taken into account self-consistently. Due to the computational expense of this method, we are limited to about 131 072 total bodies.

We modelled the early Solar system as composed by the Sun, the eight major planets, Pluto and the Kuiper belt. Each object was considered a point-mass; we did not account for collisions. The KBOs were initially moving in circular orbits in a flat ring in the plane of the ecliptic. This corresponds to an initially cold population, without a *z*-component in their motion. We adopted a surface density $\Sigma \propto r^{-2}$, where r is the heliocentric distance (see Holman 1995).

We studied two possible configurations:

(i) model A, with a radial extension in the range from 42 to 48 au and four different values of the total mass of the KB, $M = 3, 6, 1, 30\ M_\oplus$;
(ii) model B, with a radial extension in the range from 42 to 90 au and a total mass $M = 30\ M_\oplus$.

The mass function of the KBOs was derived from the conversion in mass of the size (R) distribution, assuming a constant KBO density (i.e. $\rho \sim 10^3\ \text{kg m}^{-3}$), which results in $\text{d}m/\text{d}R \propto \rho R^{-2.0\pm0.5}$ with a

cut at $m_{\min} = \frac{4}{3}\pi\rho R^3 \approx 7.0 \; 10^{-13}$ M$_\oplus$ (corresponding to $R = 1$ km) and $m_{\max} \approx 7.0 \; 10^{-4}$ M$_\oplus$ (corresponding to $R = 10^3$ km). In Fig. 2, we present the surface density of the models A and B as a function of the heliocentric distance for KBOs with the same individual mass, $m = M/N$. Here, M is the total mass of the Kuiper belt and N the number of KBOs. With this choice, we have a good sampling of the KB without an exceedingly large number ($N > 10^6$) of particles.

We integrate the equations of motion by direct summation N-body codes running on Graphics Processing Units (GPUs). For the gravitational N-body problem, these accelerators give a manifold speed increase with respect to code running on CPU (Nyland, Harris & Prins 2007; Portegies Zwart, Belleman & Geldof 2007; Bédorf & Portegies Zwart 2012). Parallel computers equipped with more than 100 GPUs have been utilized for various studies (Capuzzo-Dolcetta, Spera & Punzo 2013; Capuzzo-Dolcetta & Spera 2013; Berczik et al. 2011; Berczik, Spurzem & Wang 2013) and have been run efficiently in parallel to provide the computational power necessary to perform direct many-body simulations. Access to such large GPU-equipped supercomputers, however, is not easy, in particular when the computations required a considerable fraction of the available hardware. We therefore mainly ran our simulations on the Little Green Machine, a dedicated GPU-equipped supercomputer built at Sterrewacht Leiden, specifically for performing GPU-related calculations. Even with this machine, we had to limit the number of bodies to about a hundred thousand, but we performed several simulations (of models A and B) for each realization of the initial conditions in order to assure that the results of our calculations were not a

statistical anomaly. Recently, Portegies Zwart & Boekholt (2014) demonstrated that performing multiple simulations with the same initial conditions provide a statistically correct sampling of the real solutions. In these runs, we varied the mass, impact parameter and the inclination of the incoming star:

$$\begin{cases} M_\star = [0.5; 1; 2]\text{M}_\odot \\ \quad x = 500 & v_{x,\infty} \simeq -3, \\ \quad y = b\cos\theta & v_{y,\infty} = 0, \\ \quad z = b\sin\theta & v_{z,\infty} = 0, \end{cases} \tag{1}$$

where x, y, z are in au and velocities in km s^{-1}. The system of reference was centred on the Sun, and the impact parameters b and inclination θ characterize the orbit of the encountering star. The incoming star was placed in a ring of radius b at a distance of 500 au in the x-direction parallel to the yz-plane. In Table 1, we present the initial conditions for our simulations. In order to have a full coverage of the parameter space, $v_{y,\infty}$ and $v_{z,\infty}$ should be varied as free parameters. However, a systematic set of N-body simulations is computationally expensive (at least when considering N large enough to guarantee a good sampling) which forced us to reduce the investigation in the parameter space. Consequently, we considered that the most relevant thing to do was exploring the role of the initial yz spatial coordinates. Actually, the variation of two free parameters is enough for exploring encounters with different strength (see Section 3). Of course, a more extended study of the other free parameters could allow a wider comprehension of the role of stellar encounters on the KB structure.

Calculations were performed using the direct summation code HIGPUS (Capuzzo-Dolcetta et al. 2013), which is publicly available via the Astronomical Multipurpose Software Environment (Portegies Zwart et al. 2009, 2013; Pelupessy et al. 2013).

This code uses its own kernels to implement at best a sixth-order Hermite's integrator (Nitadori & Makino 2008) with block time-steps (Aarseth 2003) method.

We tested the accuracy of HIGPUS in getting the results of interest here through comparison with two symplectic N-body codes, NBSYMPLE (Capuzzo-Dolcetta, Mastrobuono-Battisti & Maschietti 2011), which is based on a symplectic second- and sixth-order method for the time integration of the equations of motion and HUAYNO (Pelupessy, Jänes & Portegies Zwart 2012), which uses recursive-Hamiltonian splitting to generate multiple-timestep integrators that conserve momentum to machine precision. The comparison indicates the simulations done with the (much faster) HIGPUS code as fully reliable.

All the simulations were performed using a softening parameter, ϵ, in the pairwise Newtonian potential $U_{ij} \propto \sqrt{r_{ij}^2 + \epsilon^2}$, where r_{ij} is the ith–jth particle distance. The ϵ value was set to 4×10^{-4} au, which is ~1500 times smaller than the initial average distance to the nearest neighbour in our sampling, and ~60 times bigger than the radius of Pluto. This choice guarantees the preservation of the Newtonian behaviour of the interobject force while keeping under control spurious fluctuations over the mean field (see following Section 2.1). The maximum time step for the hierarchical block time steps was ~0.02 yr. The energy conservation was checked along the system evolution by its fractional time variation, defined as

$$\left|\frac{\Delta E}{E}\right| = \left|\frac{E(t) - E(0)}{E(0)}\right|. \tag{2}$$

At the end of the simulations it was always below the value 10^{-7}, which is more than sufficient to assure that we statistically
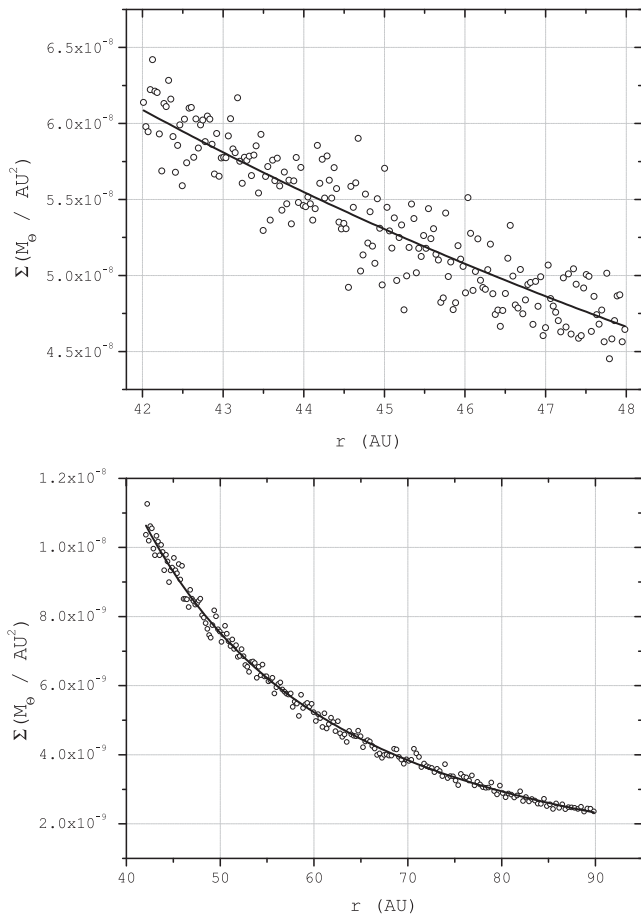
Figure 2. The initial surface density Σ of model A, with $M = 30$ M$_\oplus$ (top panel) and for model B (bottom panel).

Table 1. The initial impact parameter b and inclination θ, and position in y and z of the incoming star for each of the 64 simulations performed. The system of reference is centred at the Sun.

Index	b	θ	y(au)	z(au)	Index	b	θ	y(au)	z(au)
1	140	90	0.000	140.000	33	200	30	173.205	100.000
2	140	100	− 24.311	137.873	34	200	60	100.000	173.205
3	140	110	− 47.883	131.557	35	200	70	68.404	187.939
4	150	30	129.904	75.000	36	200	75	51.764	193.185
5	150	60	75.000	129.904	37	200	80	34.730	196.962
6	150	90	0.000	150.000	38	200	90	0.000	200.000
7	150	100	− 26.047	147.721	39	200	105	− 51.764	193.185
8	150	110	− 51.303	140.954	40	200	120	− 100.000	173.205
9	150	120	− 75.000	129.904	41	200	135	− 141.421	141.421
10	150	150	− 129.904	75.000	42	200	150	− 173.205	100.000
11	160	90	0.000	160.000	43	212.5	60	106.250	184.030
12	160	100	− 27.784	157.569	44	212.5	75	54.999	205.259
13	160	110	− 54.723	150.351	45	212.5	90	0.000	212.500
14	170	90	0.000	170.000	46	212.5	105	− 54.999	205.259
15	170	100	− 29.520	167.417	47	212.5	120	− 106.250	184.030
16	170	110	− 58.143	159.748	48	212.5	135	− 150.260	150.260
17	170	90	0.000	170.000	49	212.5	150	− 184.030	106.250
18	170	100	− 29.520	167.417	50	225	30	194.856	112.500
19	170	110	− 58.143	159.748	51	225	60	112.500	194.856
20	175	30	151.554	87.500	52	225	75	58.234	217.333
21	175	60	87.500	151.554	53	225	90	0.000	225.000
22	175	70	59.854	164.446	54	225	105	− 58.234	217.333
23	175	80	30.388	172.341	55	225	120	− 112.500	194.856
24	175	90	0.000	175.000	56	225	135	− 159.099	159.099
25	175	120	− 87.500	151.554	57	225	150	− 194.856	112.500
26	175	150	− 151.554	87.500	58	237.5	60	118.750	205.681
27	180	70	61.564	169.145	59	237.5	75	61.470	229.407
28	180	80	31.257	177.265	60	237.5	90	0.000	237.500
29	180	90	0.000	180.000	61	237.5	105	− 61.470	229.407
30	190	70	64.984	178.542	62	237.5	120	− 118.750	205.681
31	190	80	32.993	187.113	63	237.5	135	− 167.938	167.938
32	190	90	0.000	190.000	64	237.5	150	− 205.681	118.750

correctly sample the result of a true (converged) solution to the N-body problem (Portegies Zwart & Boekholt 2014).

2.1 The role of softening

The real KB is likely composed of several thousand objects. The study of the secular evolution of the KB with a high-precision, direct summation, N-body code after the encounter with a passing-by star is out of reach with our available hardware. For this reason, to represent the KBOs, we limited to values of N just below 10^4, taking as reference value $N = 2^{13} - 10 = 8182$ (10 bodies represent the incoming star, the Sun and the planets) which showed to be a good compromise between accuracy (resolution) and computational speed. Of course, to give physical reliability to our results obtained by such subsampling, we needed the introduction of a softening parameter (ϵ, as described above) whose size must be calibrated. Actually, the role of softening parameter in the N-body simulation is a long, highly debated question. It is well known that a softening parameter in the Newtonian particle–particle force has the double role of (i) avoiding the ultraviolet singularity in the closest interaction and (ii) reducing the spurious granularity effects induced by the use of a subsampled N-body set of particles to reproduce the evolution of a large stellar system. The choice of the softening length, ϵ, is characterized by a proper balance between the width of the softening length, to be small enough to preserve the Newtonian behaviour

and, at the same time, large enough to avoid spurious collisionality in the evolutionary behaviour of the system. To fulfil the second requirement above, ϵ is necessarily much larger than the average KBO radius but this is not a serious issue because the average close neighbour distance, $\langle d_{cn} \rangle$, in the simulated KB system is $\simeq 0.6$ au $\gg$ the average KB radius. On the other hand, the first requirement above (preserve Newtonian behaviour of the force) requires an ϵ sufficiently smaller than $\langle d_{cn} \rangle$. Actually, we tested the simulations with two values of the softening (4×10^{-4} and 4×10^{-5} au for ϵ), which are both significantly smaller than $\langle d_{cn} \rangle$ which is $\simeq 0.6$ au for $N = 8182$. As additional, practical, confirmation that the range of ϵ explored corresponds to reliable results, we saw that overall results remain almost unchanged with the two different choices for the ϵ value. So, we feel quite confident that our N-body results are solid in stating about KB secular evolution after the stellar encounter.
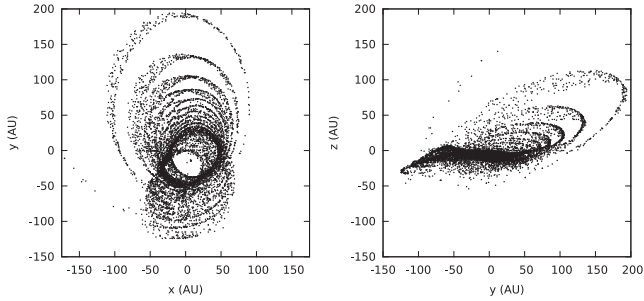
3 RESULTS

Here, we report on the results of the simulations using our two initial conditions, model A and model B.

3.1 Model A

In model A, we adopted a radial extension of the KBO between 42 and 48 au using a total mass of $M = 1, 3, 6$ and $30\,M_{\oplus}$. The mass and

Figure 3. Distribution of the $N = 8182$ KBOs in the xy-plane (left-hand panel) and in the yz-plane (right-hand panel) after an encounter with a $1\,M_\odot$ star (at $T = 3.2 \times 10^3$ yr) with parameters $b = 175$ au and $\theta = 90°$.

encounter parameters of the incoming star are presented in Table 1. The simulations are carried out until the perturbation induced by the passing star is negligible, even compared to the inter-KBO forces (the gravitational contribute on the total force on a generic KBO due

to the passing star is five magnitude lower with respect to the Sun and one magnitude comparing with the nearest KBO neighbour).

In Fig. 3, we give the distribution of the KB as obtained by model A. The figure presents the projection of the sampled system on to the xy- and the yz-planes $\sim$2500 yr after the closest approach between the Sun and the perturbing star. Some KBOs were scattered out to heliocentric distances exceeding 200 au, and with very high eccentricities, but the majority ($\sim$73 per cent) of objects remains bound. Moreover, the KBOs are distributed in over densities triggered by the passing of the star which are resonances due to the planets contribution.

In Figs 4 and 5, we show the distributions for eccentricity and inclination as a function of the semimajor axis for the KBOs from model A. Here, we varied the impact parameter parameters b and inclination θ of the encounter. The mass of the passing-by star was $1\,M_\odot$ for these simulations and the total mass of the KB was $30\,M_\oplus$. These simulations were performed with $N = 8182$ KBOs and run up to 10^4 yr.
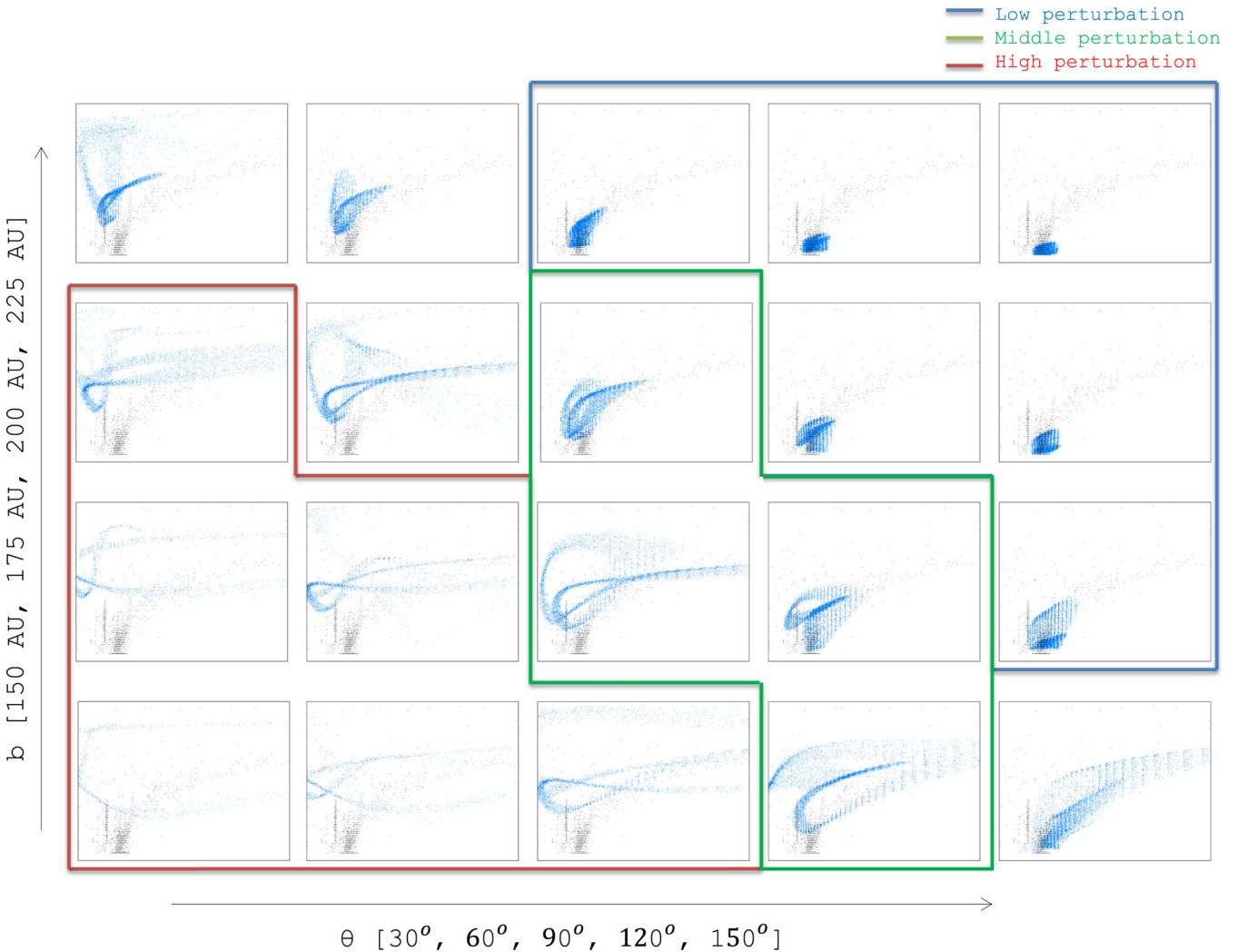
Figure 4. Parameter coverage of the eccentricities (between 0 and 1) as a function of the semimajor axis (between 35 and 100 au) for model A at 10^4 yr after the encounter. For readability we omitted the axis tickmarks and numbers, but each panel has identical axes as the images presented in the top panel of Fig. 1. The mass of the passing-by star was $1\,M_\odot$ and the total mass of the Kuiper belt was assumed equal to $30\,M_\oplus$. The black dots give the observed data from the MPC (Marsden 1980, see also Fig. 1) and the blue dots give the simulated data. Each plot has different values of parameters b and θ ordered in increasing values. We identified three regimes in which the interaction had a strong influence on the distribution of KBOs (red), moderate (green) and mild (blue).
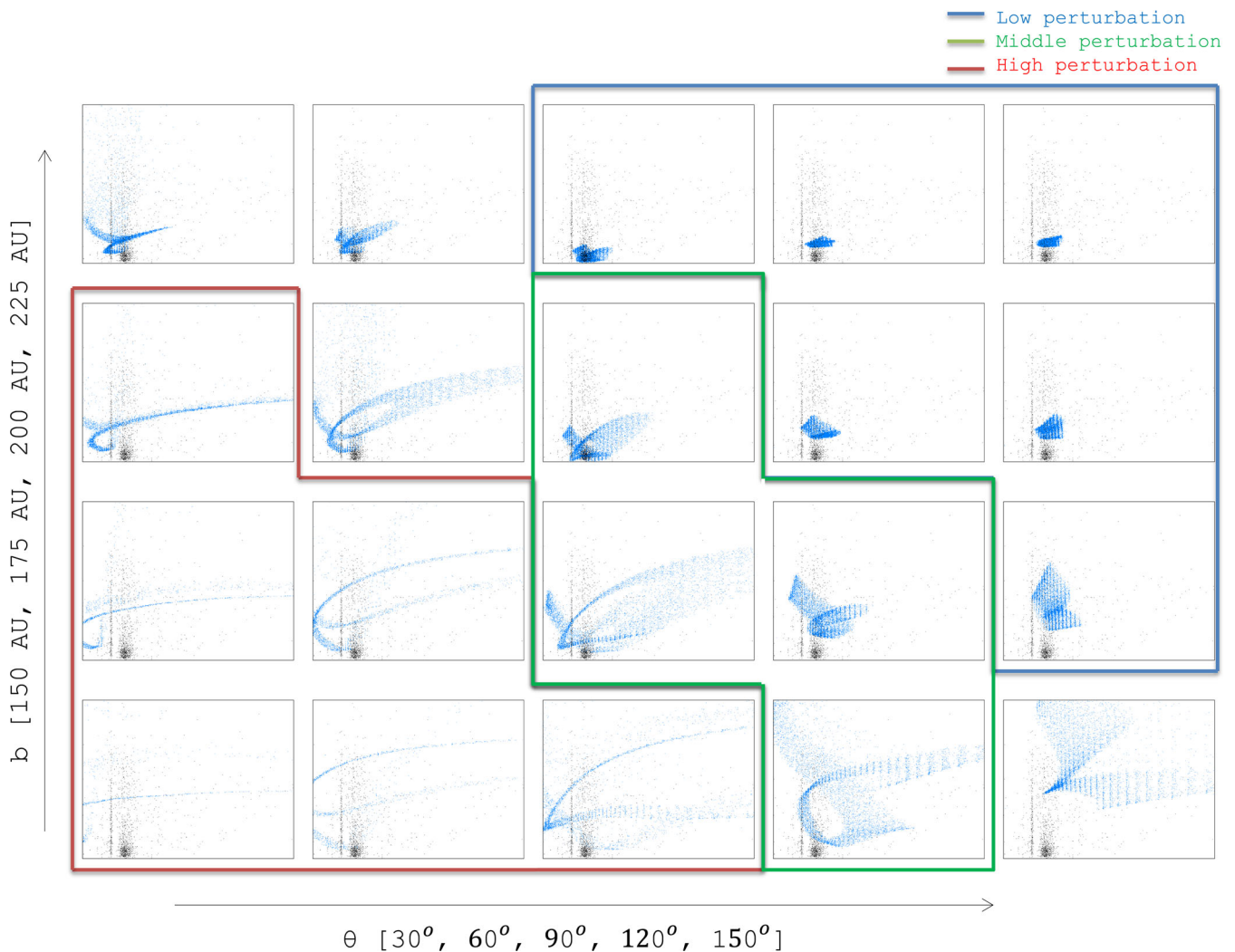
Figure 5. As Fig. 4 but then for the inclination (between 0° and 50°).

In the figures, we have identified three main regimes, which we coloured red, green and blue, indicating the highly, intermediate and relatively little perturbed system, respectively.

In the highly perturbing encounter (red zone in Figs 4 and 5), the KB is almost completely destroyed. In the moderately perturbing encounter (blue zone), the post-encounter KBO is characterized by that the majority of objects remain confined in the classical region but with slightly elevated eccentricities and inclinations. These distributions are most comparable to the observed eccentricities and inclinations in the classic (observed) regions. However, the resonant regions and the scattered region are notoriously depleted compared to the observations. In particular, the distribution in inclinations is too much concentrated around a mean value, whereas the observed inclinations are distributed more evenly between 0° and 40°.

The distribution of eccentricities in the mildly perturbed encounters (green zone in Figs 4 and 5) has almost vanished and some objects have scattered to very small semimajor axes. The general shape of the KBO, however, seems to follow the data more closely than those that result from the other more strongly perturbed interactions. The majority of bodies resides in the classical part of the KB with an extended tail of monotonically increasing eccentricities with the semimajor axis, indicating an almost constant periastron distance. On the downside, however, the distribution of inclinations is distinctively different than the observations.

We compare the distributions in eccentricities and inclinations of the KBOs at 10^4 yr after the encounter changing the total mass of the KB with values 1, 3, 6 and 30 $M_\oplus$ and the sampling of the KBOs with N in range [8182, 131 062] fixing the parameters $b = 200$ au and $\theta = 90°$. This comparison is performed using the two-dimensional Kolmogorov–Smirnov tests (K–S; Press et al. 2002). The tests give probabilities for eccentricity as well as inclination ≥ 91.2 per cent. The K–S test is a measure of the difference in the two distributions. The high values of these K–S tests are an indication that the distributions, obtained by varying the principal parameters of the sampling of the KB, show very small differences. Therefore, a small variation of the initial conditions for the KB gives rise to only small changes in final distribution, and on the short time frame of the encounter, the effect of the passing star is considerably stronger than any internal dynamical effect inside the KB. The effect the passing star has on the KB is almost impulsive, and variations in the mass of the passing star strongly affect the eccentricities and inclinations of the KBOs. These distributions therefore provide a sensitive characterization to constrain the mass and orbital parameters of the incoming star.

It may be relevant noting that some of the consequences of the encounter of star with the KB can be reliably predicted by the much simpler *test particle* approach, i.e. neglecting the internal interactions between the KBOs. Actually, a comparison of our results with test-particle simulations (Ida et al. 2000; Kobayashi & Ida 2001; Kobayashi et al. 2005; Melita et al. 2005) show a certain level of similarities:

(i) a stellar encounter pumps up strongly the eccentricities and inclinations of objects in the outer region of a planetesimal disc. Moreover, if the classical KBOs acquire high eccentricities their perihelia migrate to the inside.

(ii) a strong stellar encounter (corresponding to star passing close to the KB disc) may deplete the original, flat, KBO distribution up to 95 per cent. However, contrary to Kobayashi et al. (2005), we find that a strong depletion correspond to a full destruction of the Solar system structure. On the other hand, we found also reasonable initial encounter conditions leading to 'intermediate' cases, where a significant depletion (at about 13 per cent level) is compatible with the observed distributions of eccentricities and inclinations.

(iii) it is not possible to populate the observed resonances reproducing exactly the overdensity in the eccentricity and inclination distributions invoking only a fly-by star perturbation (see Ida et al. 2000).

The strong effect of the incoming star is clearly depicted in Figs 4 and 5. Varying the mass of the encountering star causes a migration in both b and θ. The low-mass star (0.5 M$_\odot$) gives rise to a shift to smaller values of b and θ, whereas a higher mass star (2 M$_\odot$) causes a shift towards larger values of both parameters.

The early evolution of the system strongly depends on the initial conditions of the passing star. We therefore decided to run more simulations in the middle regime (green zone) in the range $\theta = [70°, 80°, 90°]$ and $b = [170, 180, 190, 200]$ au, and in the second regime of $\theta = [90°, 100°, 110°, 120°]$ and $b = [140, 150, 160, 170]$ au. All the simulations show a characteristic tail to a monotonically increasing eccentricities; quite similar to the distribution of the eccentricities of the observed scattered KBOs. This tail is characteristic for the relatively close encounter with a stellar perturber, and we confirm the earlier made conjecture of such an encounter (Ida et al. 2000). The distribution in inclination, however, is still to be easily reproduced.

To validate our visual comparison, we performed a statistical cross-comparison between the observational and computational data for each of the simulations in Table 1 using Hotelling's two sample T^2 test (Hotelling 1931), which is a generalization of Student's t test, where

$$F = \frac{n_x + n_y - p - 1}{(n_x + n_y - 2)p} T^2 \qquad (3)$$

with F the Fisher–Snededecor random variable and T^2 is defined as

$$T^2 = \left(\bar{X} - \bar{Y}\right)^T \left[\mathbf{S} \left(\mathbf{S} \frac{1}{n_x} + \frac{1}{n_y} \right) \right] \left(\bar{X} - \bar{Y}\right), \qquad (4)$$

where $\mathbf{S}$ is the pooled sample covariance matrix of X and Y, namely,

$$\mathbf{S} = \frac{(n_x - 1)S_x + (n_y - 1)S_y}{(n_x - 1) + (n_y - 1)}, \qquad (5)$$

where S_x is the covariance matrix of the sample for X, $\bar{X}$ is the mean of the sample, and the sample for each random variable x_i in X has n_x elements, and similarly S_y is the covariance matrix of the sample for Y, $\bar{Y}$ is the mean of the sample, and the sample for each

Table 2. Values of the F indicator obtained with different parameters b (listed in the leftmost column) and θ (in the upper row) for the model A.

$b\backslash\theta$	30	60	70	80	90	100	110	120	150
225	−0.1	−0.7	–	–	−0.8	–	–	−0.9	−0.8
200	7.0	1.3	0.8	0.2	0.0	–	–	−0.7	−0.6
190	–	–	1.6	0.9	0.1	–	–	–	–
180	–	–	2.0	1.3	0.8	–	–	–	–
175	4.7	2.3	1.3	0.3	0.4	–	–	−0.6	0.0
170	–	–	–	–	0.5	0.7	−0.4	–	–
160	–	–	–	–	−0.5	0.1	−0.2	–	–
150	2.3	1.1	–	–	−0.1	0.1	−0.1	−0.3	0.1
140	–	–	–	–	−0.5	0.0	0.5	–	–

random variable y_i in Y has n_y elements. Hotelling's test states that two populations are indistinguishable if

$$F \lesssim F_{\text{tab}}(p, n_x + n_y - 1 - p, \alpha), \qquad (6)$$

where p is the number of parameters, α the significance level of the test and F_{tab} is the theoretical value of F-distribution. In Table 2, we present the values for F. Each F-value is the comparison between two samples: the observed KBOs and the computational one. In order to calculate the T^2 variable, we compute it using the JD2000 Ephemeris (right ascension and declination coordinates) of the observed KBOs and the coordinates of the computational KBOs converted in equatorial coordinates. We have normalized the values with $F_{\text{tab}}(2, N + n - 3, 0.10) = 9.491\,22$ [where we set $n_x = N$ (N is the assumed number of KBOs in the simulation) and $n_y = 1593$ is the number of observed KBOs (Marsden 1980)]. In the table (Table 2), we have subtracted one from the result to make the clearer distinction that negative values represent results for which the computational and the observational distributions are statistically indistinguishable. We did not perform Hotelling's test directly on the eccentricity and inclination distributions because the test can be calculated only on two samples that have *normal* distributions. On the other hand, (α, δ) are not independent from (e, i) values; therefore, a negative value in Table 2 gives also information about the eccentricity and inclination distributions.

This test suggests that encounters with a large impact parameter b or large inclination θ are favoured (strictly speaking, the other runs are rejected on this statistical). Although this method does not makes a distinction in quality of the results, other than accepting or rejecting it, the area of parameter space that gives small perturbations (blue zone) seems to be favoured. These simulations show a cold and low-eccentricity population of KBOs.

In Fig. 6, we present the fraction of KBOs that escaped the Solar system as a result of the stellar encounter. Based on these results, we prefer the highly scattered regime, with a low value for b and θ (red zone). In fact only in the highly perturbed regime, there is a substantial loss of mass which can reconcile the difference of 2 mag between the total mass observed and the total mass predicted by Solar system formation models (Luu & Jewitt 2002).

These contradicting results let us to perform a second series of simulations in which we adopted a wider range of semimajor axis, this we called model B.

3.2 Model B

In model B, we adopted a wider radial extension of the KBO, 42 to 90 au with a total mass of $M = 30$ M$_\oplus$. The mass and encounter parameters of the incoming star are presented in Table 1. The success of model A in reproducing the observed parameters for the KBO led
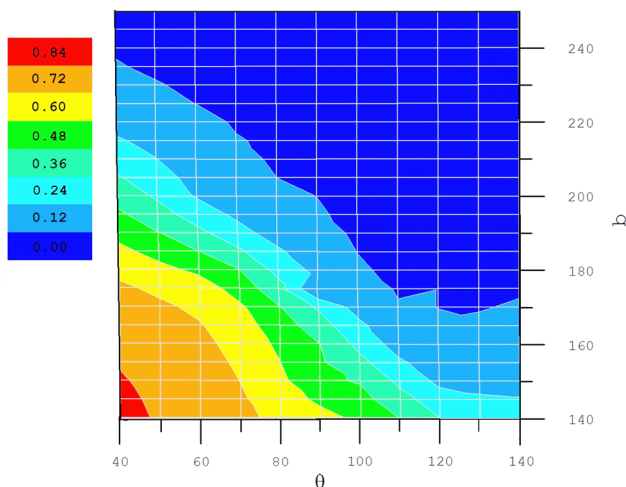
Figure 6. The 2D surface distribution of the fraction of the KBO escaped after the gravitational encounter for the model A, at $t = 10^4$ yr, in function of the parameters b and θ. In the colour map is reported for each colour the mean percentage of escaper for that zone in the parameter space.

Table 3. Values of the F indicator for various values of the parameters b (leftmost column) and θ (upper row) for the model B.

$b \backslash \theta$	60	75	90	105	120	135	150
237.5	−0.6	−0.8	−0.8	−0.9	−0.8	−0.4	−0.7
225	−0.2	−0.8	−0.6	−0.7	−0.9	−0.2	−0.7
212.5	−0.3	−0.5	−0.7	−0.7	−0.8	−0.9	−0.4
200	0.1	−0.3	−0.7	−0.8	−0.5	−0.9	−0.4

us to limit our parameter search this more extended distribution to $b = [200; 237.5]$ and $\theta = [60°; 150°]$. The results of the Hotelling test are presented in Table 3.

In Fig. 7, we present the distributions for eccentricity and inclination for $b = 200$ au and $\theta = 90°$. We determine it as the best model which gives a much better match with the observed inclinations; with value ranging from roughly $0°$ up to $40°$ in the classical regime and up to $30°$ in the scattered regime whereas the eccentricities of the scattered population and the high-eccentricity population in the classical region are consistent with the observational data. With these parameters the initial KB lost ~13 per cent of its mass in the encounter, which is quite small compared to the predictions (Luu & Jewitt 2002).

The parameters for this particular encounter has trouble reproducing the low-eccentricity population; in fact, the minimum value of the eccentricities in the classical regime 0.1. For this reason, we started a series of simulations in which we study the long-term secular evolution of the KB, on which we report in Section 3.3.

For comparison, we highlighted in Fig. 8 the eccentricities after the encounter for model A and model B for one particular encounter. For the range where the initial conditions of model A and B overlap, the post-encounter distributions in eccentricity and inclination also overlap. This supports the earlier argument that inter-KBO dynamics is not important during the encounter.

3.3 Long-term evolution

The main result for models A and B has been that an encounter in the early history of the Solar system can reproduce the high-eccentricity KB population as well as the majority of the scattered
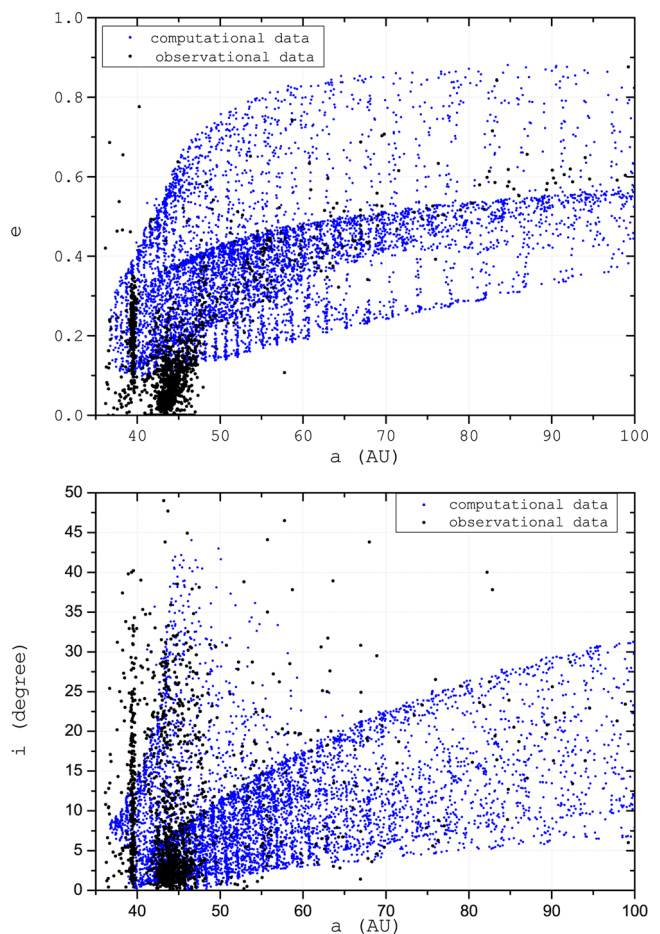

Figure 7. Comparison between the observe parameters and the result of model B directly after the scattering (at $T = 10^4$ yr) of an encounter with $b = 200$ au, $\theta = 90°$. The top panel gives the eccentricity versus the semimajor axis, the lower panel is for the inclination.

population, but the currently observed low-eccentricity population and part of the resonant populations are absent after the encounter. We will now investigate if these missing populations can be regrown by the long-term evolution of the KB.

We adopt model A with a $1 \, M_\odot$ encountering star with an impact parameter $b = 200$ au and inclination $\theta = 90°$ for this follow-up study. Ideally, we should have taken the best model B, but because the missing populations are reachable with the limited range in semimajor axes in model A, we decided that the benefit of the higher local resolution of this model outweighs the more extended width of model B. We restart the simulation at 10^4 yr after the encounter. For convenience we removed the encountering star, because it would cause numerical problems if we allowed it to continue to move further away from the Solar system, where it would no longer perturb the KB.

In Fig. 9, we present the evolution of the eccentricities and semimajor at four moments in time. This illustrates the effect of the secular evolution of the KBOs, due to their self-gravity and the influence of the planets. Whereas the encounter with the star completely removes the low-eccentricity population, the subsequent long-term evolution within the KB regrows this population. During the secular evolution, the high-eccentricity orbits contained between 37 and 46 au 'cool' to lower eccentricities. In this model, we considered 8182 KBOs ($N = 8182$) with a total mass of 30 $M_\oplus$; each KBO, then, has the mass $3.7 \times 10^{-3} \, M_\oplus$.
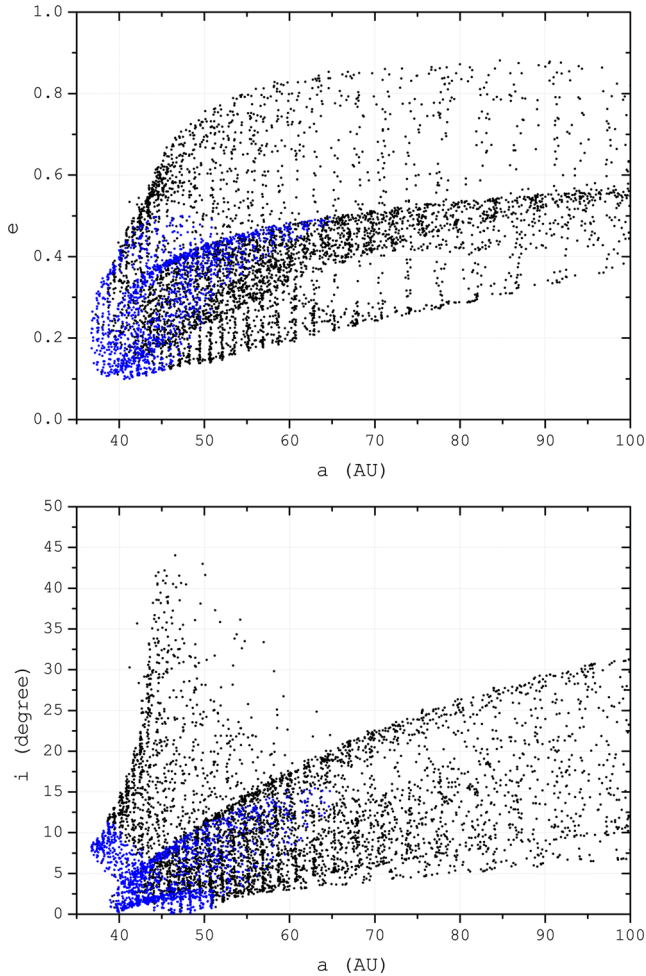
Figure 8. Distribution of eccentricities (top panel) and inclinations (bottom panel) of model A (blue) with model B (black) directly after the encounter (at $T = 10^4$ yr) with parameters $b = 200$ au and $\theta = 90°$. This comparison is to demonstrate that model A is indeed a subset of model B, but with a higher resolution at the short-period KBOs.

An important test of the importance of mutual gravitational interactions between KBOs in determining the KB secular evolution has been done through the expedient of 'switching off' the pair interaction. We saw that these simulations did not show the 'cooling' of the KB populations, with eccentricities which remained too high compared to the observations. We were driven to conclude that the mutual interactions among the KBOs are responsible of the secular evolution to the partial repopulation of the low-eccentricity distribution after a stellar encounter.

In Table 4, we present a summary of results of several simulations at varying N and the KBO radius, which correspond to a variation of the individual KBO mass. Initial conditions are those of model A. We noted that, as expected, the time needed to repopulate the low-eccentricity KBO distribution (T in the rightmost column of Table 4) scales roughly as the two-body relaxation time-scale, which, in a virialized system, has the following dependence on N and m (Binney & Tremaine 1987):

$$t_{\rm rel} \propto \frac{N}{\ln(N)} \frac{1}{\sqrt{N m}}. \tag{7}$$

After establishing the initial conditions which we considered to produce the observed KB, we run one more simulations, with

$N = 16\,374$ and a total mass of 30 $M_\oplus$ (35 per cent of the KBOs have a mass identical to Pluto, while the others have only one-fifth of this mass). The incoming 1 $M_\odot$ star approaches the Sun with impact parameter $b = 200$ au and inclination $\theta = 90°$. We continue this simulation for 0.9 Myr.

In Fig. 10, we present the energy conservation and the total number of escapers in function of time. The distribution of the eccentricities at 0.9 Myr after the encounter is shown in Fig. 11.

4 CONCLUSIONS

We investigated the effect of an encounter between a passing star on the morphology of the Kuiper belt, and its subsequent long-term evolution. Using the current morphology of the KB, we constrained the parameter of the incoming star. The orbit of the encountering star, the planets and those of the KBOs were integrated directly, as was the subsequent evolution of the internal dynamics of the KB and planets. The initial conditions for the Solar system were taken from Ito & Tanikawa (2002), and the KBOs were distributed in a flat disc between 42 and 90 au in the plane of the Ecliptic, and with a power-law density distribution with exponent −2. The total mass of Kuiper belt ranged between 1 and 30 $M_\oplus$, and the mass of the incoming star was chosen to be 0.5 1.0 and 2.0 $M_\odot$.

We compared the morphology of the KB directly after the encounter with the passing star, and after a secular evolution of up to 0.9 Myr. The best results, directly after the encounter, are obtained when the incoming star approached the ecliptic plane with an impact parameter of 170–220 au and an inclination above the Ecliptic of 60°–120°. The lower (best) values of both b and θ are for the 0.5 $M_\odot$ encountering star whereas the upper values correspond to the 2.0 $M_\odot$ intruder. We summarize these results in Table 5. In Fig. 12, we present the impact parameter and the angle θ of the incoming star as a function of its mass. A correlation between these parameters is evident and shows a degeneration in the parameters space. In fact, using different parameters is possible to reproduce an encounter with the same strength and find similar proprieties in the final KBOs distributions.

During this encounter about 13 per cent of the Kuiper belt is lost from the Solar system. Actually, results do not show a depletion of the original flat distribution up to ∼99 per cent as suggested by the observed total mass of the KB, evaluated in the range 0.3–0.1 $M_\oplus$, and the mass estimation from Solar system formation model, 30–10 $M_\oplus$ (Luu & Jewitt 2002), and match the eccentricity and inclination distributions with the observation at the same time. On the other hand, a better coverage of the initial conditions of the incoming star can very likely enhance the possibility of finding an *intermediate* case, where a strong depletion can be compatible with the observed distributions in eccentricities and inclinations.

The morphology of the high-eccentricity and scattered population of the KB are well represented directly after the encounter. The low-eccentricity population, around ∼40 au and with eccentricities ≲0.1 is almost completely absent directly after the encounter. This mismatch in the morphology can be resolved by taking the secular evolution of the Kuiper belt into account. The low-eccentricity population is reinstated within a million years. Our models did not show any particular correlation between the inclinations distributions and the mass of the KBOs. However, due to the limited number of objects in our simulations, we could run only almost single-mass particle simulations. For example in our best model the gap in mass between the two populations is only a factor of 5 and the ratio between the radii is 1.7. Due to this limitation it is not possible to constrain any significant correlations among inclination and other
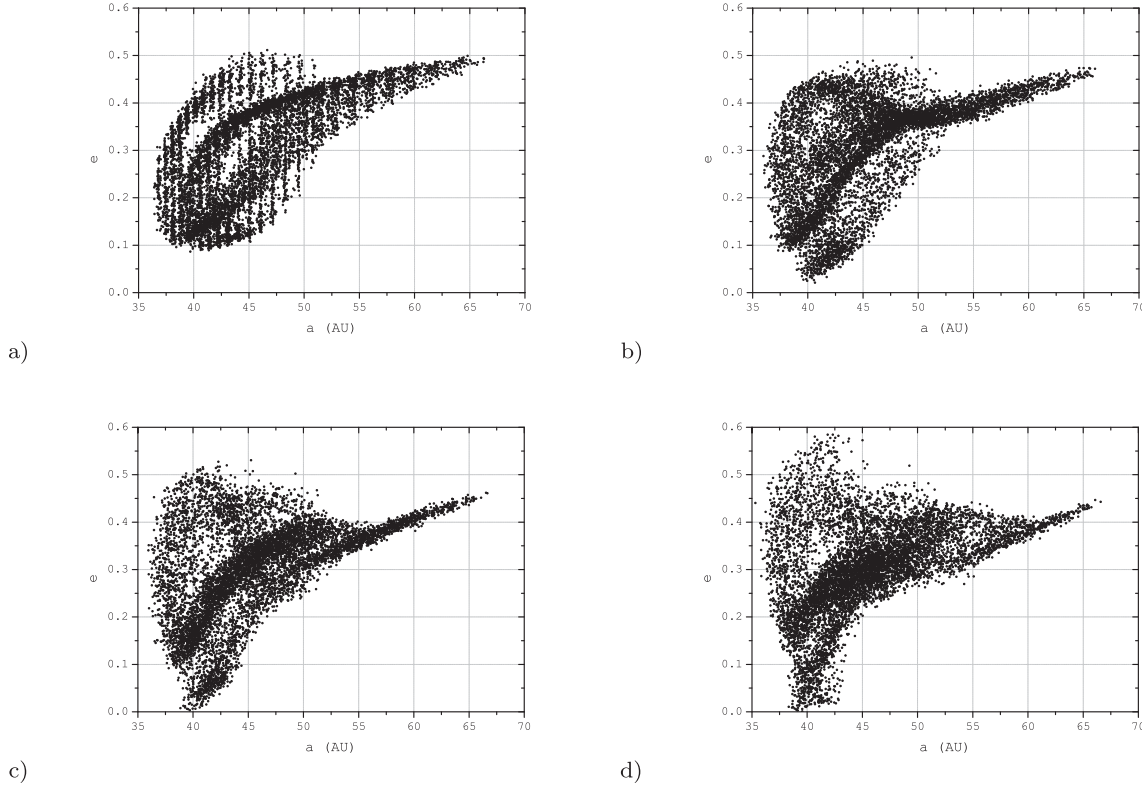
Figure 9. Time evolution of the distribution of KBOs (model A) due to the internal dynamical relaxation. The encountering star was 1 M$_\odot$, with impact parameter $b = 200$ au and inclination $\theta = 90°$. The snapshots were taken at (a) 10^4 yr, (b) 1.6×10^5 yr, (c) 3.2×10^5 yr and frame (d) at 0.5×10^6 yr.

Table 4. Entries are N, the number of KBOs; m, the mass of the single KBO, in units of Earth mass; R, the radius of the single KBO; T, the time-scale to repopulate the low-eccentricity KBO distribution. Actually, for the simulations 5–7, we checked only the initial cooling phase and then the actual values of the parameter T were extrapolated using equation (7).

Label	N	$m\,(M_\oplus)$	R (km)	T (Myr)
1	8182	3.7×10^{-3}	1741	0.50
2	8182	3.7×10^{-4}	808	1.58
3	8182	3.7×10^{-5}	375	5.00
4	4086	3.7×10^{-3}	1741	0.77
5	65 526	3.7×10^{-3}	1741	1.15
6	65 526	3.7×10^{-4}	808	3.64
7	81 820	7.0×10^{-7}	100	91.56

properties, such as the size distribution of the KBOs and the number of KBO binaries. In conclusion, the sampling limiting our model and the relatively short time-scale of our simulations cannot give reliable results on that (actually, our finest simulation involved 16 384 KBOs and was carried up to 0.9 Myr).
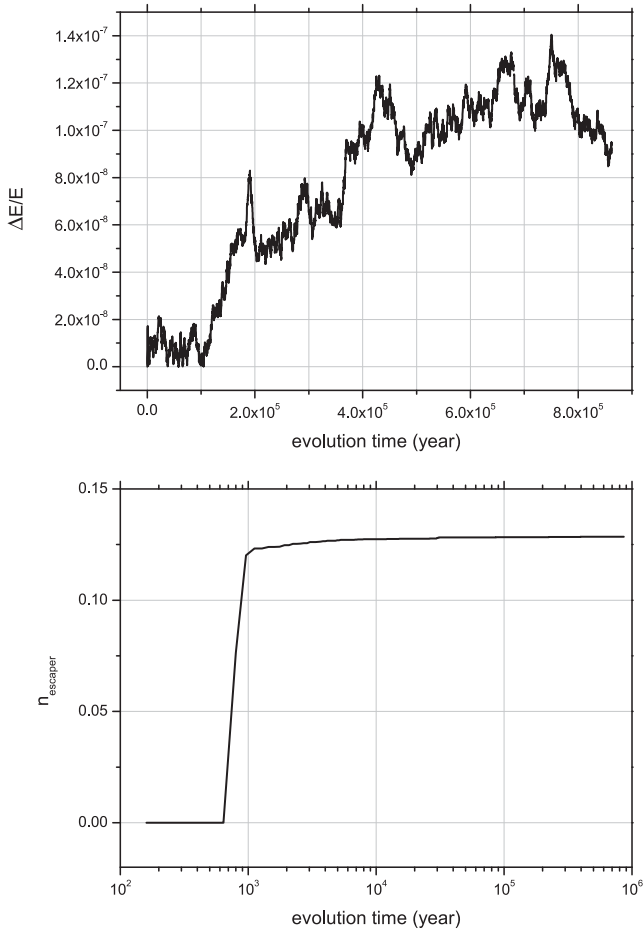
We expect that a more sophisticated investigation of the long-term ($\sim$100 Myr) evolution of the KB, with a proper population over the whole KBO mass spectrum will show the 'relaxation' of the eccentricities to low values as it happens in the case of mass monodisperse-particle simulations. Such detailed studies would thus provide important information about the final distribution of the KBOs, which will allow a complete comparison with observable

such as the size–inclination relation, but unfortunately it is hard to achieve at the moment without the access to a very large GPUs cluster.

While the secular evolution repopulated the low-eccentricity population, it triggered the further KB causing the depletion of the resonant population, which was initiated by the passing star. This loss of the resonant population can be due to the insufficient sampling of the KB in our simulations. Alternatively, the early migration of the planets is driving the repopulation of the resonant families (Malhotra 1995; Ida et al. 2000). Such planetary reordering would be a natural consequence of the Nice model (Levison et al. 2008). Moreover, the resonances, that we have suddenly after the passage of the fly-by star, do not show an eccentricity and inclination distributions compatible with the observations.

Figure 10. The relative error in the energy ($|\Delta E/E|$) (top panel) and the fraction of escapers (bottom panel) as functions of time for a 1 M$_\odot$ encounter with $b = 200$ au and $\theta = 90°$.
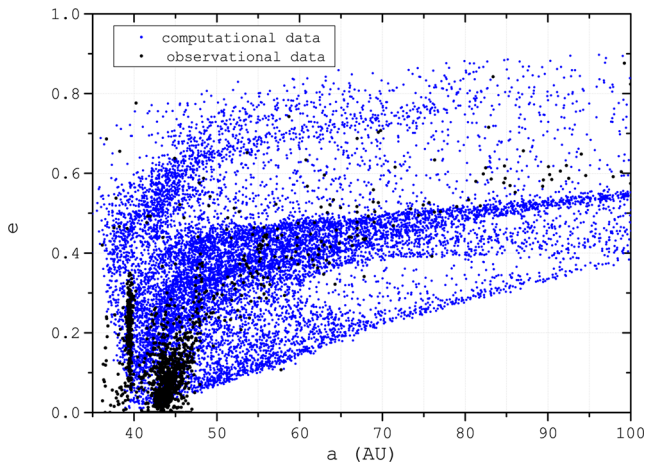
Figure 11. The eccentricities of the model B with encounter parameters $b = 200$ au and $\theta = 90°$ at 0.9 Myr. The black dots are the observed data from the MPC (Marsden 1980) and the blue ones are the simulated data using our best model.

Table 5. The optimal encounter parameters (b and θ) obtained for a star with mass M (in solar masses) approaching with velocity at infinity of 3 km s^{-1} the Solar system (model B). The units of b and θ are those adopted in this paper.

M	0.5	1.0	2.0
b	170	200	220
v_∞	3	3	3
θ	60	90	120
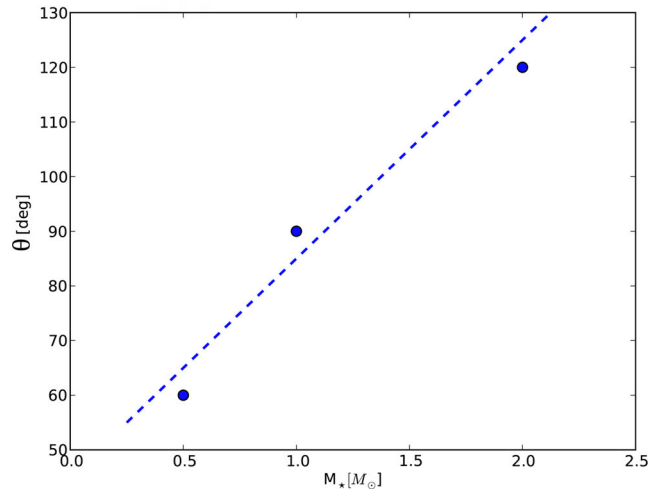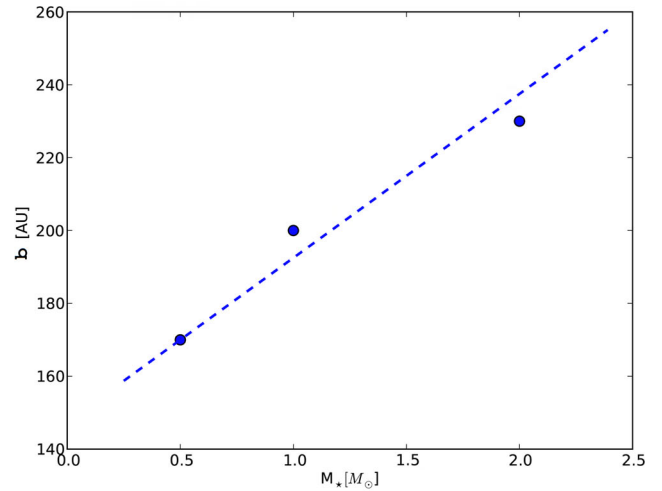
Figure 12. The impact parameter b (top) and inclination θ (bottom) as a function of the mass of the incoming star for our most favourite model (see Table 5). The dashed line gives a fit to the tree points to indicate the trend, which follows $b = 170 + 45(M - 0.5)$ for the impact parameter and $\theta = 65 + 40(M_\star - 0.5)$ for the inclination.

in Amsterdam and by. We finally thank M. Spera for his help in porting the code to various architectures.

REFERENCES

Aarseth S. J., 2003, Gravitational N-Body Simulations. Cambridge Univ. Press, Cambridge

Bédorf J., Portegies Zwart S., 2012, Eur. Phys. J. Spec. Top., 210, 201

Berczik P., Spurzem R., Wang L., 2013, 3rd Int. Conf. on High Performance Computing, HPC-UA 2013, Up to 700k GPU Cores, Kepler, and the Exascale Future for Simulations of Star Clusters Around Black Holes. p. 52, available at: http://hpc-ua.org/hpc-ua-13/proceedings/

Berczik P. et al., 2011, Int. Conf. on High Performance Computing, HPC-UA 2011, High Performance Massively Parallel Direct N-body Simulations on Large GPU Clusters. p. 8 available at: http://hpc-ua.org/hpc-ua-11/proceedings/

Bernstein G. M., Trilling D. E., Allen R. L., Brown M. E., Holman M., Malhotra R., 2004, AJ, 128, 1364

Binney J., Tremaine S., 1987, Galactic dynamics. Princeton Univ. Press, Princeton, NJ

Brown M. E., 2001, AJ, 121, 2804

Brucker M. J., Grundy W. M., Stansberry J. A., Spencer J. R., Sheppard S. S., Chiang E. I., Buie M. W., 2009, Icarus, 201, 284

Capuzzo-Dolcetta R., Spera M., 2013, Comput. Phys. Commun., 184, 2528

Capuzzo-Dolcetta R., Mastrobuono-Battisti A., Maschietti D., 2011, New Astron., 16, 284

Capuzzo-Dolcetta R., Spera M., Punzo D., 2013, J. Comput. Phys., 236, 580

Doressoundiram A., Boehnhardt H., Tegler S. C., Trujillo C., 2008, Color Properties and Trends of the Transneptunian Objects. Univ. Arizona Press, Tucson, AZ, p. 91

Fraser W. C., Kavelaars J. J., 2009, AJ, 137, 72

Gomes R. S., 2003, Icarus, 161, 404

Holman M. J., 1995, in Kinoshita H., Nakai H., eds, 27th Symp. on Celestial Mechanics, The Distribution of Mass in the Kuiper Belt. Tokyo, Japan, p. 116

Hotelling H., 1931, Ann. Math. Stat., 2, 360

Ida S., Larwood J., Burkert A., 2000, ApJ, 528, 351

Ito T., Tanikawa K., 2002, MNRAS, 336, 483

Jewitt D., Luu J., 1993, Nature, 362, 730

Kenyon S. J., Luu J. X., 1999, AJ, 118, 1101

Kobayashi H., Ida S., 2001, Icarus, 153, 416

Kobayashi H., Ida S., Tanaka H., 2005, Icarus, 177, 246

Levison H. F., Stern S. A., 2001, AJ, 121, 1730

Levison H. F., Morbidelli A., Van Laerhoven C., Gomes R., Tsiganis K., 2008, Icarus, 196, 258

Luu J. X., Jewitt D. C., 2002, A&A, 40, 63

Malhotra R., 1993, Nature, 365, 819

Malhotra R., 1995, AJ, 110, 420

Malmberg D., Davies M. B., Heggie D. C., 2011, MNRAS, 411, 859

Marsden B. G., 1980, Celest. Mech., 22, 63

Melita M. D., Larwood J. D., Williams I. P., 2005, Icarus, 173, 559

Nitadori K., Makino J., 2008, New Astron., 13, 498

Noll K. S., Grundy W. M., Stephens D. C., Levison H. F., Kern S. D., 2008, Icarus, 194, 758

Nyland L., Harris M., Prins J., 2007, Fast N-Body Simulation with CUDA, Addison-Wesley, Boston, p. 677

Pelupessy F. I., Jänes J., Portegies Zwart S., 2012, New Astron., 17, 711

Pelupessy F. I., van Elteren A., de Vries N., McMillan S. L. W., Drost N., Portegies Zwart S. F., 2013, A&A, 557, A84

Portegies Zwart S. F., 2009, ApJ, 696, L13

Portegies Zwart S., Boekholt T., 2014, ApJ, 785, L3

Portegies Zwart S. F., Belleman R. G., Geldof P. M., 2007, New Astron., 12, 641

Portegies Zwart S., McMillan S. L. W., van Elteren E., Pelupessy I., de Vries N., 2013, Comput. Phys. Commun., 183, 456

Portegies Zwart S. et al., 2009, New Astron., 14, 369

Press W. H., Teukolsky S. A., Vetterling W. T., Flannery B. P., 2002, Numerical Recipes in C++: The Art of Scientific Computing. Cambridge Univ. Press, Cambridge

Volk K., Malhotra R., 2011, ApJ, 736, 11

This paper has been typeset from a TEX/LATEX file prepared by the author.